CHAPTER

4 Understanding the nonlinear physiological and behavioral effects of tDCS through computational neurostimulation

James J. Bonaiuto[1], **Sven Bestmann**

Sobell Department of Motor Neuroscience and Movement Disorders, UCL Institute of Neurology, University College London, London, UK

[1]Corresponding author: Tel: +44 (0) 20 3 448 8769; Fax: +44 (0) 207 278 9836, e-mail address: j.bonaiuto@ucl.ac.uk

Abstract

Despite the success of noninvasive brain stimulation (NIBS), the mechanism of action through which different stimulation techniques interact with information processing in targeted neural circuits largely remains unknown. Applying neurostimulation *in silico* to computational models with biophysical plausibility provides one route to interrogate the possible mechanisms through which stimulation interacts with neural circuits, and generate predictions about the resultant behavior. Here, we address the recent observation that the physiological and behavioral effects of transcranial direct current stimulation (tDCS) might be nonlinear with regard to stimulation intensity or duration. We simulate neurostimulation in an established, biophysically informed neural network attractor model that generates simple behavioral choices and thus allows for assessing the impact of stimulation on both neural dynamics and behavior. We demonstrate that nonlinear effects of stimulation intensity on the accuracy and decision time of the model can arise from a limit on the integration rate of the network, nonlinear effects of stimulation on neural firing rates before the onset of the stimulus, and the inhibitory effect of hyperpolarizing stimulation on pyramidal neurons. We thus present a detailed modeling treatment of nonlinear tDCS effects during a behavioral task, and provide detailed hypotheses about the neural causes that lead to observed nonlinear behavioral effects during stimulation. This framework can provide a blueprint for future work on the neural and behavioral consequences of NIBS in health and disease.

Keywords

Transcranial direct current stimulation, Neural attractor model, Biophysical model

Progress in Brain Research, Volume 222, ISSN 0079-6123, http://dx.doi.org/10.1016/bs.pbr.2015.06.013

1 INTRODUCTION

Noninvasive electrical stimulation of the human brain has become a staple technique for investigating causal structure–function relationships, functional mapping, and promoting lasting physiological change in both health and disease. Despite the success of noninvasive brain stimulation (NIBS), the mechanism of action through which different stimulation techniques interact with information processing in targeted neural circuits remains unknown. Indeed, there is a startling paucity of mechanistic explanations on how stimulation affects physiology, and how this in turn changes the computations specific circuits carry out (Bestmann et al., 2015; de Berker et al., 2013). Consequently, how a given stimulation protocol ought to change behavior often remains subject to speculation. Moreover, devising novel and better stimulation regimes, in particular for translational purposes, often relies on an exercise of trial and error. These issues partly arise from a lack of biologically informed models that provide mechanistic explanations or hypotheses about the impact of NIBS on the information processed in neural circuits, the emerging properties of complex neural systems, and resultant consequences on behavior.

In this chapter, we illustrate how such models can be used *in silico* to interrogate how specific physiological and behavioral outcomes of NIBS might be generated by neural systems. We focus on a specific example: recent observations suggest that the physiological and behavioral effects of a neuromodulatory NIBS technique, transcranial direct current stimulation (tDCS), might be nonlinear with regard to stimulation intensity or duration (Paulus et al., 2013). tDCS utilizes surface electrodes to apply weak electrical currents to the brain, and induces changes in cortical and subcortical excitability. Experiments typically vary the polarity of the stimulation (anodal vs. cathodal) applied over a presumed target brain region. We here refer to this distinction as depolarizing or hyperpolarizing stimulation according to the theorized effect of each stimulation type on pyramidal neurons. The effects of tDCS are commonly framed in a sliding-scale rationale whereby cortical excitability is dialed up or down with increasing stimulation intensity (Nitsche and Paulus, 2000, 2011), though as we will demonstrate here this simple heuristic likely eschews the complex interactions of widespread polarization on the dynamics of neural circuits (Bestmann et al., 2015).

Indeed, many existing conceptual models of the effects of tDCS remain unsatisfactory for several reasons (Bestmann et al., 2015; de Berker et al., 2013). First, many conceptual models are typically simplistic to the point of triviality. For example, the simple sliding-scale rationale is commonly put forth as an explanation for the neural effects of tDCS, and stipulates that anodal or cathodal stimulation increases or decreases the overall activity in a brain region, with a predictable (one-to-one) mapping onto the behavioral consequences (e.g., Krause et al., 2013). Ignoring network dynamics, such a view overlooks interactions between different subpopulations of neurons within a region that may be affected differently by stimulation (e.g., due to their morphology or orientation). Critically, there is no mechanistic explanation as to how

neural polarization ought to result in behavioral outcomes that would justify a sliding-scale rationale, i.e., they make no reference to the changes in the information that is processed within targeted brain regions or networks. Second, many existing conceptual models are unsatisfactory in that they oversimplify how stimulation might affect the emergent properties of neural circuits, and how this would then translate to behavioral change. Intuition is an unreliable indicator of the effect of currents on networks of thousands of neurons of varying morphology and function. For example, widespread polarization of pyramidal cells in a cortical region is likely to have direct or downstream effects on inhibitory interneurons, which in turn will influence the pattern of activity in the pyramidal cells.

Moreover, and with relevance to this chapter, the observation of nonlinear effects questions the generalizability of such sliding-scale models. These effects include ceiling effects on cortical excitability (Kuo et al., 2013) and performance in a working memory task (Hoy et al., 2013), as well as a reversal of effects. For example, the effect of hyperpolarizing stimulation reduces cortical excitability at 1 mA but enhances it at 2 mA (Batsikadze et al., 2013), and depolarizing stimulation can reduce excitability when applied for longer durations (Monte-Silva et al., 2013).

The fact that tDCS, and indeed other types of NIBS, can cause nonlinear effects at the neurophysiological and behavioral level also poses a problem both for determining the appropriate stimulation dosage and for developing a causal understanding of its effects. Such effects could be the result of physical laws governing the conductance of electrical currents, physiological properties of the affected neurons, or emergent properties of the neural circuits they are a part of. For example, possible explanations for nonlinear stimulation outcomes that have been put forward include differences in synaptic plasticity induced by stimulation-triggered calcium influx (Batsikadze et al., 2013), but also heterogeneity in effective dosage and regions targeted by stimulation across participants (Bikson et al., 2012; Datta et al., 2012).

This chapter thus develops a mechanistic explanation for possible nonlinear neural and behavioral effects of tDCS, by using *in silico* neurostimulation of an established, biophysically plausible neural network attractor model. Computational modeling approaches of the kind discussed here complement experimental investigations by simulating the emergent network dynamics that neural circuits can exhibit. These emergent properties can be difficult or even impossible to predict without consultation of biophysically informed generative models, and commonly used conceptual models are largely insufficient for generating satisfactory explanations for observed experimental effects (Bestmann et al., 2015). Computational models with sufficient biological plausibility can thus bridge the gap between stimulation and behavior by simulating the changes in neural activity that mediate between the two. The use of such models is indeed now common in other fields of neuroscience (Bonaiuto and Arbib, 2010; Christopoulos et al., 2015; Itti and Koch, 2001; Riesenhuber and Poggio, 2000; Wolpert and Ghahramani, 2000), yet strikingly few such approaches have been adopted for the field of NIBS.

We will start by introducing a biophysical attractor model (Wang, 2002) which has been successfully used to explain behavioral choices, but also neural firing rate changes during behavior (Compte et al., 2000; Wang, 2008), population measures such as BOLD (Bonaiuto and Arbib, 2014) and MEG response during choice behavior (Hunt et al., 2012). The model comprises two stable attractor states corresponding to different choice options. Task-related inputs and background noise modulate the state of the network until it settles in one of the stable attractor states, representing a decision. We then describe how one can simulate the impact of tDCS on such a network. We detail how *in silico* neural polarization can generate predictions about the consequences of tDCS on neural dynamics in a neural decision network, and how this ought to affect the resulting accuracy and speed of behavioral responses generated by this network. Both behavioral measures emerge naturally from the model and are determined by the attractor state that the model settles into and the speed at which it attains that state. We then address the issue of nonlinear effects by submitting the network to tDCS manipulations of different stimulation intensities, and show that many nonlinear effects can be gracefully explained by the emergent properties of the network.

To summarize, we provide a detailed example on how computational neurostimulation can provide a framework for interrogating how NIBS alters the dynamics in neural circuits, how such effects influence and alter the information processed within the circuit, and how this may translate into changes in accuracy and speed of perceptual choices.

2 A BIOPHYSICALLY INFORMED NEURAL NETWORK MODEL OF DECISION MAKING

2.1 MODEL ARCHITECTURE

The neural network attractor model contains two populations of pyramidal cells, one for each response option, and one population of inhibitory interneurons (Bonaiuto and Arbib, 2014; Hunt et al., 2012; Wang, 2002, 2008). Each pyramidal population receives a different task-related input encoding the value of some variable relevant to the task (for example, the evidence accumulated for the available choice options; Wang, 2002). In our variant of this model, two populations of pyramidal neurons (p1 and p2, 800 neurons each) receive task-related inputs, excite neurons in the same population via reciprocal projections, and mutually inhibit each other via a common pool of 400 inhibitory interneurons which are also reciprocally connected (Fig. 1). The pyramidal populations form excitatory synapses (AMPA and NMDA) on target cells and the interneuron population form inhibitory synapses on its targets. The ratio of excitatory to inhibitory cells is 4:1 (Bonaiuto and Arbib, 2014; Braitenberg and Schüz, 1991; Izhikevich, 2006; Mayor and Gerstner, 2005).

Input to the pyramidal cells in each population can be separated into task-related input and background noise. Task-related input comes in the form of spikes

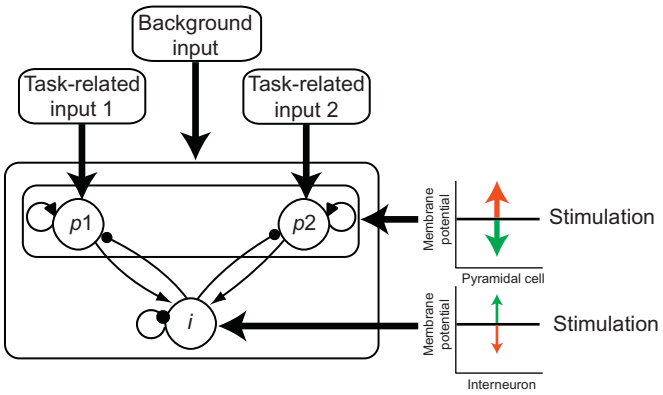

FIGURE 1

Model architecture. The model contains two pyramidal cell populations, p1 and p2, which have recurrent excitatory connections and inhibit each other via a single interneuron population, i, which has recurrent inhibitory connections. All populations receive excitatory background input from a common source, and the two pyramidal populations additionally receive excitatory task-related inputs. Simulation of tDCS-induced currents is implemented in the form of depolarizing or hyperpolarizing currents which modulate the membrane potential and are parameterized separately for pyramidal and interneuron populations.

generated from Poisson spike generators which represent the output of other brain regions on a given trial. For the purpose of this chapter, these inputs are varied by changing the difference between the input firing rates to the two pyramidal populations while keeping the total input firing rate equal. We here refer to *contrast* as the ratio of the difference between these inputs and their sum. This contrast is analogous to the difference in evidence favoring one decision over another. Difficult trials are then defined by trials in which each input fires at approximately the same rate, while easy trials can be defined as those in which one input fires at a high rate while the other fires at a very low rate. In all trials, the total input to the network was set to 80 Hz.

Nontask-related (background) input arrives to each pyramidal cell and interneuron through a common set of spike inputs from a single Poisson distribution at a set rate. As a result, the neurons fire spontaneously at a low rate comparable to neocortical pyramidal cells (Swadlow, 1990, 1994). We instantiated the model with different background input firing rates sampled from a range typically used in similar models (here 890–950 Hz, Wang, 2002; Liu and Wang, 2008; Deco and Rolls, 2005).

The mean population firing rates are obtained by convolving the instantaneous firing rate with a Gaussian filter with 5 ms width. After applying the task-related inputs to the network, the firing rates of the pyramidal populations converge to a pattern in which differences in the inputs are magnified. This winner-take-all dynamic is due to the reciprocal connectivity and structure of the network and is a common feature of neural network attractor models with bistable attractor states (Camperi and

Wang, 1998; Wilson and Cowan, 1972). As the firing rate of one population increases, it exerts an increasingly inhibitory influence on the other population via the inhibitory interneurons that connect the two. This further perpetuates the increasing activity of the dominant population as the inhibitory drive supplied by the other dwindles as activity falls. The dynamics of the model result in the firing rate of one pyramidal population (typically the one receiving the strongest input) continuing to increase, while the firing rate of the other population decreases to approximately 0 Hz. In order to analyze the behavioral output of the network, we consider a response option to be *selected* when the corresponding pyramidal population exceeds a set *response threshold* of 25 Hz.

2.2 SYNAPSE AND NEURON MODEL

In the following, we provide a detailed account of the architecture of the attractor model used here. Synapses are modeled as exponential (AMPA, $GABA_A$), or biexponential conductances for slower rising synapses (NMDA). Exponentially decaying conductances are governed by the following equation:

$$g(t) = G\mathrm{e}^{-t/\tau},$$

where G is the maximal conductance (or weight) of that specific synapse and τ is a synapse type-specific decay time constant.

Similarly, biexponential synaptic conductances are given by

$$g(t) = G\frac{\tau_2}{\tau_2 - \tau_1}\left(\mathrm{e}^{-t/\tau_1} - \mathrm{e}^{-t/\tau_2}\right),$$

where τ_1 and τ_2 are synapse type-specific decay and rise time constants. Synaptic currents are generated using these conductances and the associated reversal potential, E:

$$I(t) = g(t)(V_\mathrm{m} - E),$$

where V_m is the membrane voltage. The additional voltage dependence of NMDA synapses is captured by

$$I_\mathrm{NMDA}(t) = \frac{g_\mathrm{NMDA}(t)(V_\mathrm{m} - E_\mathrm{NMDA})}{1 + \left[\mathrm{Mg}^{2+}\right]\exp(-0.062V_\mathrm{m})/3.57},$$

where $[Mg^{2+}]$ is the extracellular magnesium concentration.

The synaptic currents of each type (AMPA, NMDA, and $GABA_A$) are summed, and the total synaptic current is injected as the input into the adaptive exponential leaky integrate-and-fire (LIF) neural model (Brette and Gerstner, 2005):

$$I_\mathrm{total}(t) = I_\mathrm{AMPA}(t) + I_\mathrm{NMDA}(t) + I_{\mathrm{GABA_A}}(t)$$

$$C\frac{dV_m}{dt} = g_L(V_m - E_L) + g_L\Delta_T e^{\frac{V_m - V_T}{\Delta_T}} + I_{total},$$

where C is the membrane capacitance, g_L is the leak conductance, E_L is the resting potential, Δ_T is the slope factor (which determines the sharpness of the voltage threshold), and V_T is the threshold voltage. After emitting a spike, the membrane potential is reset to V_R and a refractory period, τ_R, is enforced during which neurons cannot emit another spike. Connections between neurons within and between populations are initialized probabilistically. Axonal conductance delays are implemented with delays of 0.5 ms. Neural and synaptic parameter values are taken from the literature where possible and set empirically otherwise (Table 1; Hestrin et al., 1990; Jahr and Stevens, 1990; Salin and Prince, 1996; Spruston et al., 1995; Xiang et al., 1998).

Connection probabilities between the neural populations are set empirically in order to induce winner-take-all dynamics (Bonaiuto and Arbib, 2014). The probability that each pyramidal cell projected to an AMPA or NMDA synapse on other pyramidal cells in the same population was 0.08, and that each inhibitory interneuron projected to a $GABA_A$ synapse on other interneurons in the same population was 0.1. Pyramidal cells of each population formed AMPA or NMDA synapses on the inhibitory interneurons with probability 0.1, and each inhibitory interneuron exhibited $GABA_A$ synapses on the pyramidal cells with probability 0.2. The large-scale connectivity between populations was therefore fixed, but the connectivity between individual neurons in those populations was randomly generated according to the connection probability parameters.

2.3 SIMULATING tDCS-INDUCED CURRENTS IN A NEURAL NETWORK MODEL

We here simulate the effects of tDCS by simply adding an additional current to the pyramidal cells and inhibitory interneurons, based on values from simulations reproducing tDCS-induced changes in sensory-evoked potentials *in vivo* (Molaee-Ardekani et al., 2013) and current understanding of the mechanism of action of tDCS (Bikson et al., 2004; Bindman et al., 1964; Funke, 2013; Nitsche and Paulus, 2011; Radman et al., 2009; Rahman et al., 2013). Specifically, depolarizing (anodal) stimulation was simulated by adding depolarizing current into each pyramidal cell and hyperpolarizing current into each interneuron, while hyperpolarizing (cathodal) current was simulated by adding hyperpolarizing current into pyramidal cells and depolarizing current into interneurons. Pyramidal cells and interneurons were stimulated with opposite polarities based on modeling work which showed that this pattern of stimulation is required to reproduce sensory-evoked potentials *in vivo* (Molaee-Ardekani et al., 2013) and a consideration of the effects of stimulation on neurons at different spatial orientations (Radman et al., 2009). The input to each adaptive exponential LIF neuron thus became

$$I_{total}(t) = I_{AMPA}(t) + I_{NMDA}(t) + I_{GABA_A}(t) + I_{stim}(t),$$

where $I_{stim}(t)$ is the current representing tDCS at time i.

Table 1 Parameter values for the neural model used in the simulations

Parameter	Description	Value
$G_{AMPA(ext)}$	Maximum conductance of AMPA synapses from external inputs	2.1 nS (pyramidal cells) 1.62 nS (interneurons)
$G_{AMPA(rec)}$	Maximum conductance of AMPA synapses from recurrent inputs	0.05 nS (pyramidal cells) 0.04 nS (interneurons)
G_{NMDA}	Maximum conductance of NMDA synapses	0.165 nS (pyramidal cells) 0.13 nS (interneurons)
$G_{GABA\text{-}A}$	Maximum conductance of $GABA_A$ synapses	1.3 nS (pyramidal cells) 1.0 nS (interneurons)
τ_{AMPA}	Decay time constant of AMPA synaptic conductance	2 ms
$\tau_{1\text{-}NMDA}$	Decay time constant of NMDA synaptic conductance	2 ms
$\tau_{2\text{-}NMDA}$	Rise time constant of NMDA synaptic conductance	100 ms
$\tau_{GABA\text{-}A}$	Decay time constant of $GABA_A$ synaptic conductance	5 ms
$[Mg^{2+}]$	Extracellular magnesium concentration	1 mM
E_{AMPA}	Reversal potential of AMPA-induced currents	0 mV
E_{NMDA}	Reversal potential of NMDA-induced currents	0 mV
$E_{GABA\text{-}A}$	Reversal potential of $GABA_A$-induced currents	−70 mV
C	Membrane capacitance	0.5 nF (pyramidal cells) 0.2 nF (interneurons)
g_L	Leak conductance	25 nS (pyramidal cells) 20 nS (interneurons)
E_L	Resting potential	−70 mV
Δ_T	Slope factor	3 mV
V_T	Voltage threshold	−55 mV
V_s	Spike threshold	−20 mV
V_r	Voltage reset	−53 mV
τ_r	Refractory period	2 ms (pyramidal cells) 1 ms (interneurons)

During stimulation trials, this current was applied for the duration of each trial, starting with trial onset. We thus only consider here the acute effects of varying stimulation intensity and their possible nonlinear effects on physiology and behavior. To this end, we varied the magnitude of the injected current from 0.25 to 8 pA, but in line with previous simulations the magnitude of injected current into interneurons was always half of that applied to pyramidal cells (Molaee-Ardekani et al., 2013). We performed additional simulations in which stimulation was only applied to the pyramidal populations, but we note that the results were qualitatively similar (see Section 3). Relative to no stimulation, the injected current changed the resting membrane potential of each neuron by a small amount. This change in membrane potential varied from −0.4 mV with −8 pA injected current to 0.4 mV with 8 pA injected current. This is within the range found by *in vitro* studies of the effects of tDCS (Bikson et al., 2004; Radman et al., 2009; Rahman et al., 2013).

2.4 MODELING OF INTENSITY-DEPENDENT CHANGES ON NEURAL DYNAMICS AND BEHAVIOR

To illustrate how computational neurostimulation can inform understanding of the consequences of tDCS, we here generated 20 virtual subjects and assessed the effects of stimulation in each subject, under six different input contrast levels (20 trials at each contrast level). The sum of the two task-related inputs always equaled 80 Hz (at contrast = 0 both inputs were at 40 Hz, and contrast = 1 both one input was at 80 Hz and the other at 0 Hz), so the total strength of the input received by the network remains equal across all conditions. Each trial lasted for 4 s, with task-related input applied from 1 to 3 s. This procedure was repeated for control (no stimulation), depolarizing, and hyperpolarizing stimulation conditions, respectively, and at each tested level of *stimulation intensity*.

In all stimulation conditions, stimulation was applied for the entire duration of the simulation: prior to and during the task-related inputs. We refer to the task-related input corresponding to the winning pyramidal population (the population whose firing rate first reaches the response threshold of 25 Hz) as the *selected input*, and the input to the other population as the *unselected input*. The *decision time* for each trial is here set as the earliest time at which the selected pyramidal population's firing rate reaches the response threshold of 25 Hz. Accuracy of the model's performance can be defined as the percentage of trials in which the selected input corresponds to the stronger task-related input. Comparison of the *accuracy threshold* allows for assessing the impact of stimulation intensity. Accuracy threshold was here defined as the contrast level required for a virtual subject to attain 80% accuracy.

One important feature of the model is that on many trials, one pyramidal population spontaneously fires at a slightly higher rate than the other even before the onset of the task-related input, due to the noisy background input to both populations. We refer to this difference in the firing rates of the pyramidal populations as the *prestimulus bias*.

2.5 MODEL IMPLEMENTATION AND ANALYSES OF MODEL BEHAVIOR

All our simulations were implemented in the Python programming language using the Brian simulator v1.4.1 (Goodman and Brette, 2008). Behavioral data of virtual subjects and mean firing rates of the model were analyzed using R v2.14.1 (R Development Core Team, 2011). We report two-way ANOVA tests for the main effects of stimulus condition (depolarizing or hyperpolarizing) and intensity as well as their interaction on each measured variable. Pairwise *t*-tests (Bonferroni corrected) were conducted between the stimulation conditions at each stimulation intensity level where a significant interaction effect was detected. Regressions were run using the *Z*-score of each independent variable, and in the case of decision speed, of the dependent variable as well.

2.5.1 Intensity-Dependent Impact of tDCS on Accuracy Thresholds

Without applying any stimulation, the mean accuracy threshold of the present model was 0.063 (SD = 0.006). This corresponds to one task-related input firing at 42.4 Hz and the other at 37.6 Hz. As we show below, both stimulation (i.e., tDCS) polarity and stimulation intensity have profound impact on this accuracy threshold.

For currents resulting in net depolarization (resembling anodal stimulation), increasing stimulation intensity raises the accuracy threshold, relative to control. In other words, for the specific process captured by the model used here, depolarizing currents impair behavioral accuracy, and this effect is furthermore intensity dependent. By contrast, the relative accuracy threshold decreases during hyperpolarization. Model accuracy thus improves under hyperpolarizing currents (Fig. 2C and Table 2). As shown in Fig. 2, even with relatively low currents, a different effect of depolarizing and hyperpolarizing stimulation on thresholds starts to emerge.

As can be seen in Fig. 2, for depolarizing currents the effect on accuracy thresholds increases monotonically with stimulation strength. However, for hyperpolarizing stimulation, the accuracy threshold decreases initially but then begins to reverse and increase again at higher intensities. Closer inspection of the underlying network behavior reveals that the probability of the firing rates of either pyramidal population to reach the response threshold (here: 25 Hz) during difficult trials decreases at higher hyperpolarizing currents. In extreme, this means that no response is emitted at all (Fig. 3A), and indeed, the percentage of trials without a response thus sharply increases at a stimulation intensity of 6 pA (Fig. 3B). The present model thus provides a putative mechanistic explanation for nonlinear stimulation effects on accuracy thresholds: at low intensity levels, hyperpolarization can dampen the effects of background noise, but when stimulation intensity increases the net effect of tDCS might be a profound slowing of the network dynamics such that the network does not elicit a behavioral response at all. Our simulations used a fixed response threshold of 25 Hz, but simulations suggest that response thresholds might be adaptively tuned through synaptic plasticity (Lo and Wang, 2006). Not only would a modulation in response threshold alter the behavioral predictions for this model, but also synaptic

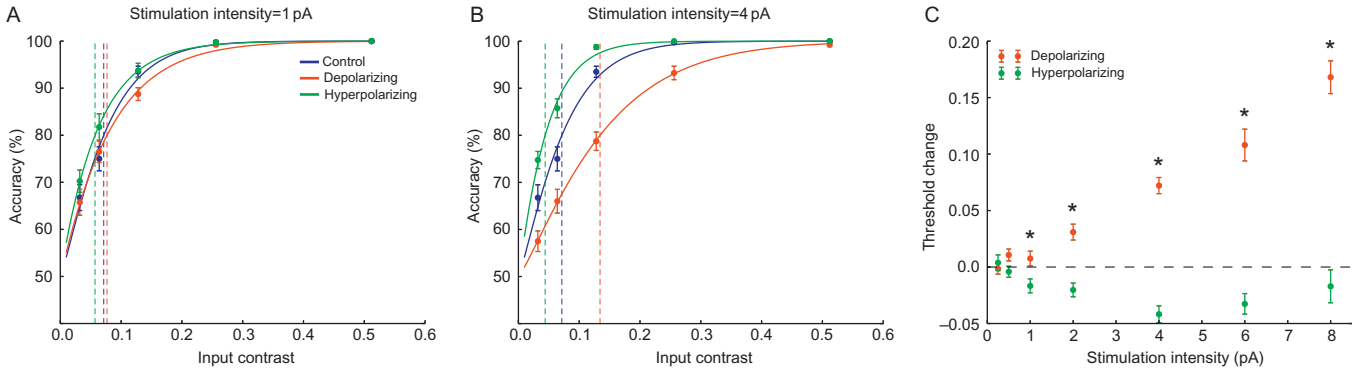

FIGURE 2

Effects of stimulation on model accuracy. (A) Accuracy as a function of input contrast with stimulation intensity of 1 pA. Compared to control (blue (black in the print version)), hyperpolarizing stimulation shifts the threshold to the left, improving performance, and depolarizing stimulation shifts the threshold to the right, reducing performance. (B) Same as (A) with stimulation intensity at 4 pA. The effect of stimulation on accuracy is more pronounced at the higher stimulation intensity level. (C) The difference in accuracy thresholds between stimulation and control, as a function of stimulation condition and intensity. Depolarizing stimulation monotonically increases this difference and therefore reduces performance. Hyperpolarizing stimulation decreases the difference in accuracy thresholds, leading to improved performance. Asterisks indicate where pairwise comparisons between de- and hyperpolarizing stimulation are significant. Notably, the effect of hyperpolarizing stimulation is nonlinear with regard to stimulation intensity. Following performance increases at lower stimulation intensities (1–4 pA), at higher current intensities (4–8 pA) performance decreases (although still superior to the control condition).

Table 2 Statistics for all two-way ANOVAs

	Stimulation condition		Stimulation intensity		Stimulation condition × intensity	
Measure	***F*(1,17)**	***p***	***F*(6,17)**	***p***	***F*(6,17)**	***p***
Change in accuracy threshold	233.850	1.166×10^{-38}	103.563	7.301×10^{-21}	182.081	3.270×10^{-32}
Percent of trials with no response	40.646	7.638×10^{-10}	70.871	2.100×10^{-15}	73.577	7.086×10^{-16}
Decision time difference slope	1249.739	1.775×10^{-104}	17.857	3.239×10^{-5}	1037.409	1.730×10^{-95}
Prestimulus bias	726.009	2.990×10^{-79}	1656.321	5.769×10^{-30}	641.274	6.008×10^{-74}
Slope of prestimulus bias – selection sigmoid	0.454	0.501	1.287	0.258	1.370	0.243
Prestimulus bias – decision time offset	780.579	2.662×10^{-82}	22.579	3.254×10^{-6}	822.571	1.238×10^{-84}
Prestimulus bias – decision time slope	3.180	0.076	0.430	0.513	0.069	0.793
Accuracy logistic regression – prestimulus bias coefficient	179.240	7.751×10^{-32}	74.331	5.243×10^{-16}	186.660	8.226×10^{-33}
Accuracy logistic regression – input contrast coefficient	27.102	3.774×10^{-7}	7.210	0.008	17.208	4.466×10^{-5}
Decision speed linear regression – prestimulus bias coefficient	11.446	0.001	105.966	3.031×10^{-21}	0.286	0.593
Decision speed linear regression – input contrast coefficient	604.711	1.661×10^{-71}	61.654	9.119×10^{-14}	303.700	2.205×10^{-46}

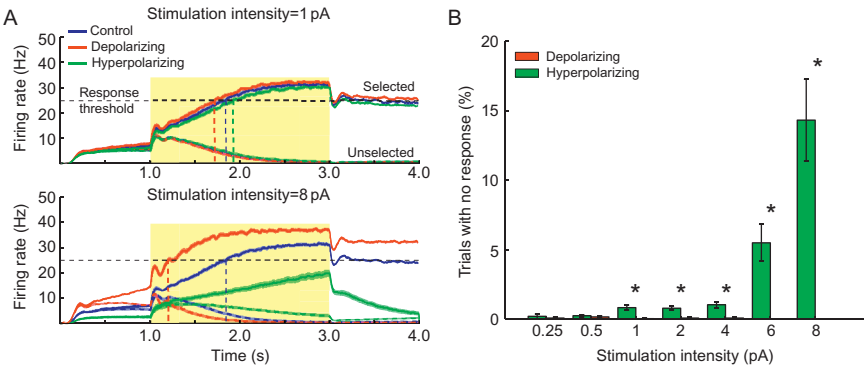

FIGURE 3

Response omissions caused by stimulation explain the nonlinear effects on accuracy caused by hyperpolarization. (A) The mean firing rate of the pyramidal populations for both stimulation conditions at 1 pA (top) and 8 pA (bottom) during trials with low input contrast (difficult trials). The shaded area depicts the duration of the task-related inputs and the dotted vertical lines show the time at which the mean firing rate of the selected pyramidal population reaches the response threshold. During high-intensity (8 pA) hyperpolarization, neither pyramidal population reaches the 25 Hz response threshold. (B) The percentage of trials with no response as a function of stimulation condition and intensity. Asterisks indicate where pairwise comparisons between de- and hyperpolarizing stimulation are significant. The percentage stays at about 0 for depolarizing stimulation, but begins to increase with hyperpolarizing stimulation at around −6 pA stimulation intensity, thus explaining the reversal in performance improvement seen in Fig. 2.

plasticity is modulated by tDCS (Fritsch et al., 2010), further complicating conceptual models of tDCS effects and underscoring the need for computational modeling.

One implication of this result is that the assumption of a linear scaling with stimulation intensity which is often implicit in applications of tDCS (Iyer et al., 2005; Ohn et al., 2008; Shekhawat et al., 2013) may not hold in complex dynamic networks such as the one used here (and indeed even more complex systems such as the brain). We will return to this point later on.

2.5.2 Intensity-Dependent Impact of tDCS on Decision Times

The results above pinpoint a possible mechanism underlying changes in the accuracy of performance during tDCS, and how nonlinear effects of stimulation intensity on accuracy can arise from the dynamics of neural attractor networks. Stimulation of the same network, however, can also affect the speed with which a network reaches a decision. In other words, by focusing on either the accuracy or the speed of the network decision, different outcomes can be observed, much like focusing on either the speed or the accuracy of subject's choices when conducting experiments *in vivo*.

As expected (Palmer et al., 2005), the decision time of the network always decreases with increasing input contrast (Fig. 4A and B). In other words, when input

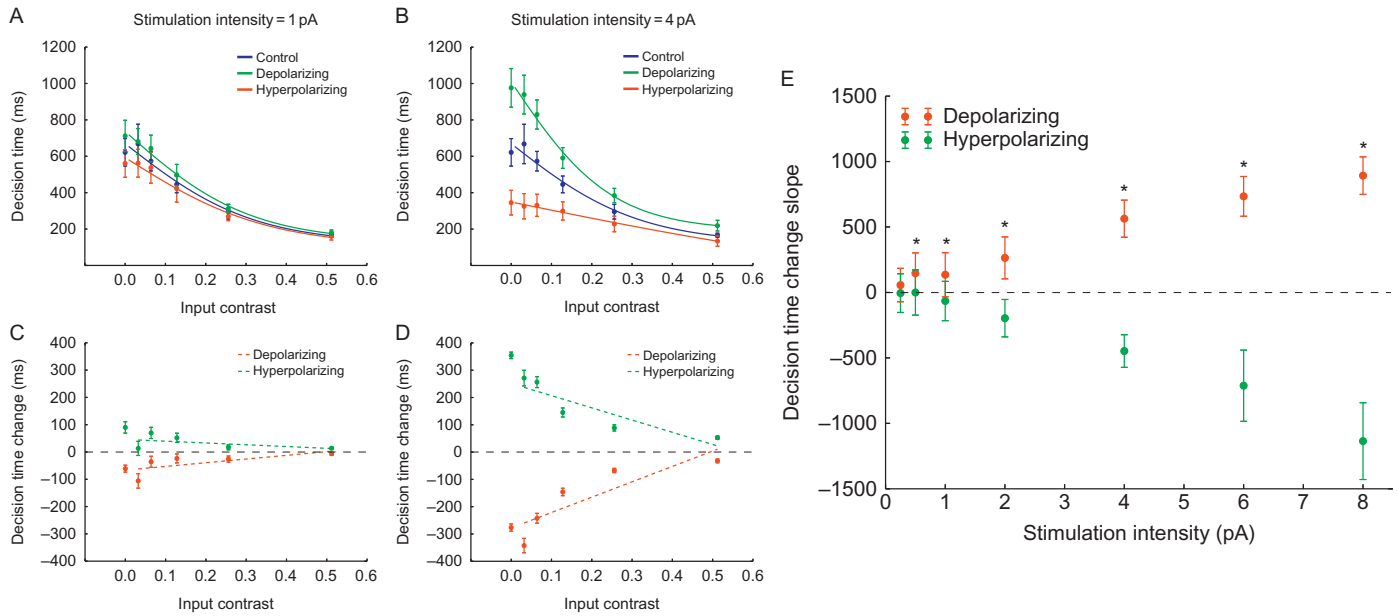

FIGURE 4

Effects of stimulation condition and intensity on decision time. (A, B) Decision time as a function of input contrast for stimulation intensity (A: 1 pA; B: 4 pA). In all conditions, decision time decreases with increasing input contrast. Hyperpolarizing stimulation increases decision times, while depolarizing stimulation decreases decision times. (C, D) The difference between decision times during stimulation and no stimulation, as a function of input contrast at stimulation intensity = 1 pA (C) and 4 pA (D). At low input contrast, high-intensity stimulation amplifies this difference, whereas stimulation even at 8 pA cannot overcome the influence of large input contrast values. (E) The slope of the fitted linear function to decision time differences as a function of stimulus intensities. Asterisks indicate where pairwise comparisons between de- and hyperpolarizing stimulation are significant. There is a ceiling effect on depolarizing stimulation because there is a limit to how fast the network can converge on a decision.

contrast is low the network simply requires more time before one population "wins" over the other and the network reaches a stable state. At each contrast level, the difference between the mean decision time during each stimulation condition and the control condition can be fitted to a linear function, as shown in Fig. 4.

Depolarizing stimulation applied to the network *in silico* reduces decision time at low input contrast levels, whereas hyperpolarizing stimulation increases it. In both stimulation conditions, however, this difference gradually disappears with increasing input contrast (Fig. 4C and D). Put simply, during trials with high input contrast, the network is already near the lower bound of the decision time which is determined by neural time constants and population dynamics. Consequently, externally applied perturbations of the system, at least within the ranges tested here, do not overcome the stable attractor state that the network quickly reaches under such circumstances. In other words, these simulations predict that behavior should be unaffected on "no brainer" trials in which strong inputs provide unequivocal evidence for one response over the other. We entertain the idea that in some studies, null results may not be the consequence of inefficient stimulation *per se*, but that instead for the selected experimental conditions tDCS cannot sufficiently perturb the neural trajectory from stimulus to decision to action.

However, as shown in Table 2, the slope of the relationship between the input contrast and decision time difference increases with depolarizing and decreases with hyperpolarizing stimulation. This means that the effect of stimulation on more difficult trials (i.e., with low input contrast) is amplified relative to easier ones (trials with high input contrast), and this difference is further amplified by increasing stimulation intensity. A nonlinear ceiling effect on the relationship between depolarizing stimulation intensity and decision time can then occur because of the lower bound on the decision time. Because there is a limit to the speed at which the network can reach one of its stable states, increasingly larger perturbations from depolarizing stimulation have diminishing effects on decision time in difficult trials. As with accuracy, interrogation of the emergent properties of the model thus provides a possible mechanism for nonlinear effects of tDCS on decision time.

2.5.3 Impact of Stimulation Intensity on Neural Dynamics

One advantage of the type of network models such as the one employed here is that they allow for flexible interrogation of the neural dynamics under different experimental manipulations. These cannot be easily observed empirically in human participants. Modeling the potential dynamics of neural circuits during stimulation can thus help to generate hypotheses about the changes in firing dynamics under different stimulation conditions, which in turn would be amenable to be tested experimentally in invasive recording experiments.

As can be seen in Fig. 5, prior to the onset of the task-related inputs, each pyramidal population in our model fires at approximately 5 Hz and the interneuron population fires at about 1 Hz, due to the stochastic background input received by these populations. This difference in baseline firing rates is not critical to the model's behavior. With slightly different connection strengths and levels of background input,

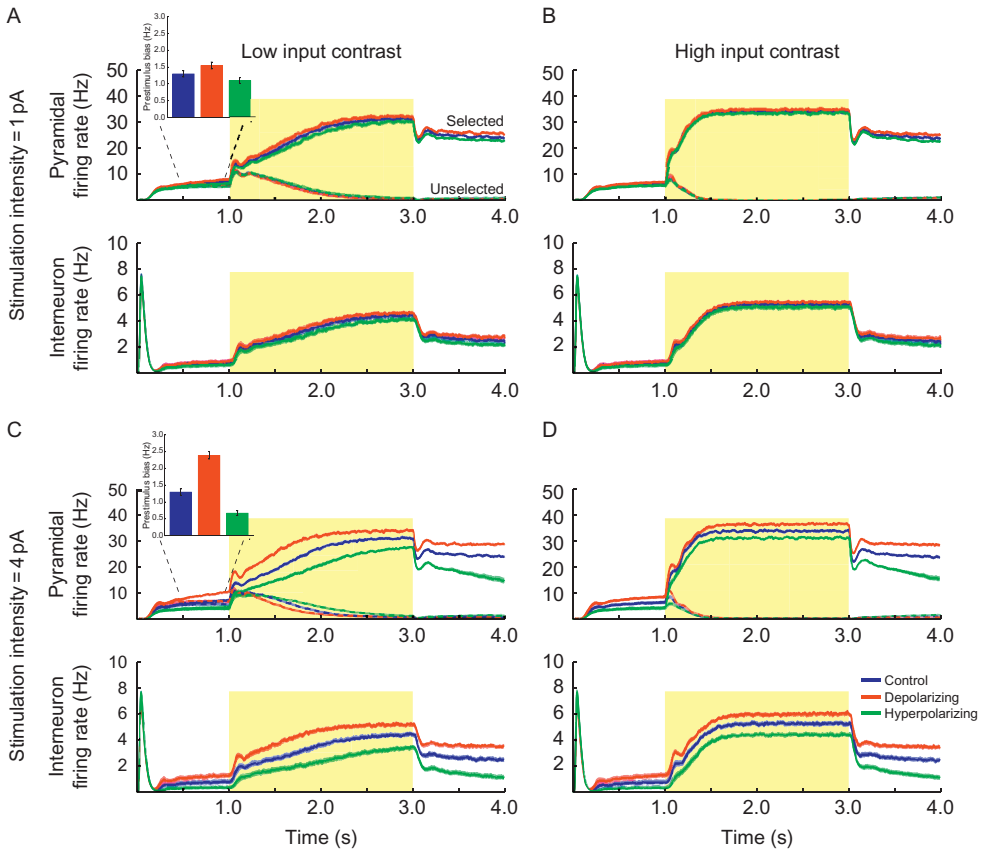

FIGURE 5

Mean neural population firing rates for different stimulation intensities and input contrasts. Mean firing rates for pyramidal cell populations (top plot of each panel) and the inhibitory interneuron population (bottom plot of each panel). Shaded regions represent the duration of task-related inputs. Insets show the mean difference in pyramidal population firing rates between the different stimulation conditions, before the onset of the task-related stimulus. (A) Stimulation intensity = 1 pA, minimum input contrast. (B) Stimulation intensity = 1 pA, maximum input contrast. (C) Stimulation intensity = 4 pA, minimum input contrast. (D) Stimulation intensity = 4 pA, maximum input contrast.

the neural populations spontaneously fire at different rates, but the network dynamics remain qualitatively similar. The task-related input then causes an initial increase in firing rate in both pyramidal populations, which in turn increases the excitatory drive to the interneuron population. The recurrent excitatory projections within each pyramidal population cause the firing rate of the winning population to continue to increase at a higher rate (due to receiving more task-related input), which in turn further excites the interneuron population. The interneuron population inhibits both pyramidal populations but this has a larger effect on the population that receives less task-related input and therefore less recurrent excitation. Consequently, the network eventually reaches a stable state, in which one pyramidal population exhibits high sustained firing rates, whereas the firing rate of the other pyramidal population converges toward 0 Hz (Fig. 5).

When sorting the pyramidal population firing rates of each trial based on which population was selected and which was unselected, prior to onset of task-related input the selected pyramidal population fires, on average, at a slightly higher rate than the unselected population. Because all neurons receive background (nontask-related) input at the same rate, this effect can be attributed to random fluctuations in the amount of noisy background input. We refer to this difference in firing rate prior to the onset of the task-related input as prestimulus bias.

Critically, because stimulation was applied throughout the entire simulation similar to common practice in tDCS experiments, depolarizing network stimulation amplifies this bias, whereas hyperpolarizing stimulation suppresses it (insets in Fig. 5A and C). Moreover, as shown in Fig. 6, the prestimulus bias increases with increasing depolarizing stimulation intensity and decreases with increasing hyperpolarizing stimulation intensity (Fig. 6C and Table 2). We point out that with the model architecture used here, nonlinear floor effects on the prestimulus bias can occur with hyperpolarizing stimulation at high intensities. Because prestimulus bias is measured as a difference between the firing rates of the pyramidal populations, and stimulation abolishes this difference, there is a natural lower limit on the prestimulus bias.

2.5.4 Effect of Prestimulus Bias on Selection Accuracy

The former observation is relevant because prestimulus bias has a significant impact on the emerging dynamics of the network when task-related inputs are received. In trials with a large prestimulus bias, the pyramidal population with the higher initial firing rate is much more likely to win the competition, irrespective of it receiving the stronger task-related input, simply because of the initial head-start endowed by the prestimulus bias. This effect is magnified in trials with low input contrast because the difference in the task-related inputs is not strong enough to overcome the prestimulus bias. By contrast, large input contrasts ought to overcome prestimulus biases. Consequently, one may expect nonlinear effects on the resultant network behavior when contrasting different stimulation intensities that amplify or dampen prestimulus biases to different degrees.

The relationship between the prestimulus bias and the percent of trials in which the biased population was selected can be fit to a sigmoid function (Fig. 6A and B).

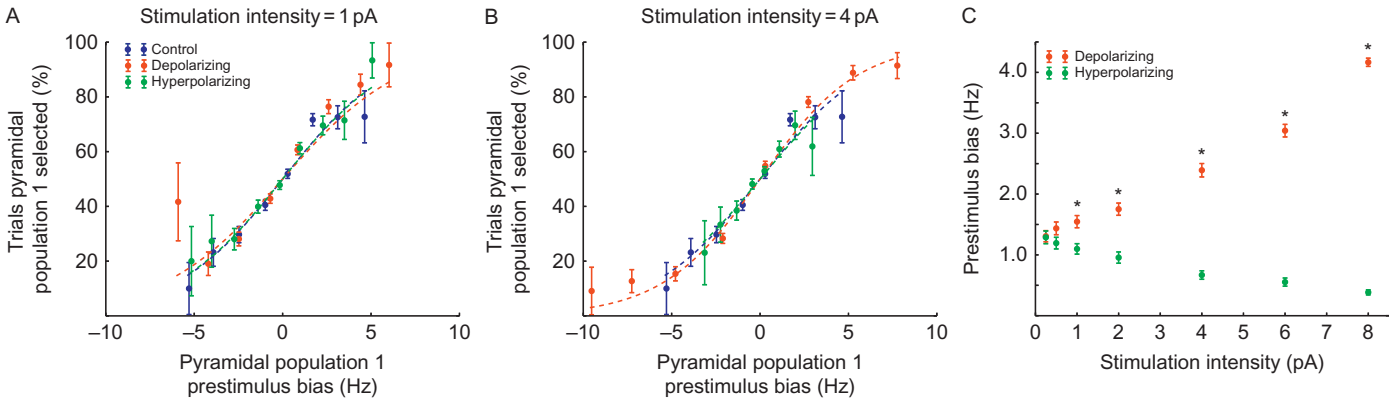

FIGURE 6

Prestimulus bias. The percentage of trials in which pyramidal population 1 was selected as a function of the prestimulus bias (negative = bias to population 2, positive = bias to population 1) at stimulation intensity = 1 pA (A) and 4 pA (B). While the range of prestimulus bias values changes with stimulation condition and intensity, the effect on the selection remains constant. (C) The prestimulus firing rate bias as a function of stimulation condition and intensity. Asterisks indicate where pairwise comparisons between de- and hyperpolarizing stimulation are significant. The bias steadily increases with depolarizing stimulation and decreases with hyperpolarizing stimulation. There is a floor effect during hyperpolarizing stimulation as the difference in the firing rates of the pyramidal populations approaches 0 Hz.

However, this analysis reveals that the steepness parameter of this function is not affected by stimulation condition, or intensity, or their interaction (Table 2). Therefore, while stimulation affects the *range* of prestimulus bias values (Fig. 6C), the effect of the prestimulus bias *per se* on the selection behavior of the model remains constant throughout the conditions. This means that under the stimulation intensities tested here, once the task-related inputs are received, accuracy is a function of the contrast between those inputs and the prestimulus bias initially induced by noise and amplified or dampened by stimulation.

2.5.5 Effect of Prestimulus Bias on Decision Time

As one may expect, prestimulus bias also has an effect on the decision time. Across all stimulation conditions, the decision time decreases with increasing prestimulus bias. In other words, a large prestimulus bias means that one pyramidal population reaches the response threshold faster.

Figure 7A and B shows the linear relationship between the prestimulus bias and decision time for the control, depolarizing, and hyperpolarizing stimulation conditions and stimulation intensities of 1 and 4 pA, respectively. The slope reflects the difference between the firing rate of the biased pyramidal population and the response threshold when the task-related input begins, while the offset represents the mean decision time when the prestimulus bias is zero. When the prestimulus bias is larger, the biased pyramidal population is slightly closer to the response threshold, reducing the time needed to reach it. However, the slope of this function is not affected by stimulation condition, or intensity, or their interaction (Table 2). The offset increases with increasing hyperpolarizing stimulation intensity and decreases with increasing depolarizing stimulation intensity (Fig. 7C and Table 2). The difference in the offset shows that the effects of stimulation extend beyond the prestimulus period (stimulation is applied throughout the duration of the simulation). Even when the prestimulus bias is the same across stimulation conditions, the mean decision time is shorter for depolarizing stimulation and longer for hyperpolarizing stimulation because the stimulation is amplifying (depolarizing) or dampening (hyperpolarizing) the effects of the bias even after the onset of the task-related input.

2.5.6 Influence of Prestimulus Bias and Input Contrast on Selection

To determine the relative influence of prestimulus bias and input contrast on accuracy, a logistic regression on accuracy using the *Z*-scored prestimulus bias and input contrast as the independent variables reveals that input contrast is a better predictor of network accuracy than prestimulus bias, under all conditions with stimulation at 1 pA (Fig. 8A). However, at 4 pA simulated depolarizing stimulation increases the relative influence of prestimulus bias on accuracy, while hyperpolarizing stimulation reduces it (Fig. 8B). For depolarizing stimulation, the influence of the prestimulus bias on accuracy increased with stimulation intensity (Fig. 8C). This is because at higher stimulation intensities the prestimulus bias is quite large (Fig. 6), and if the network is biased in the wrong direction the input contrast is

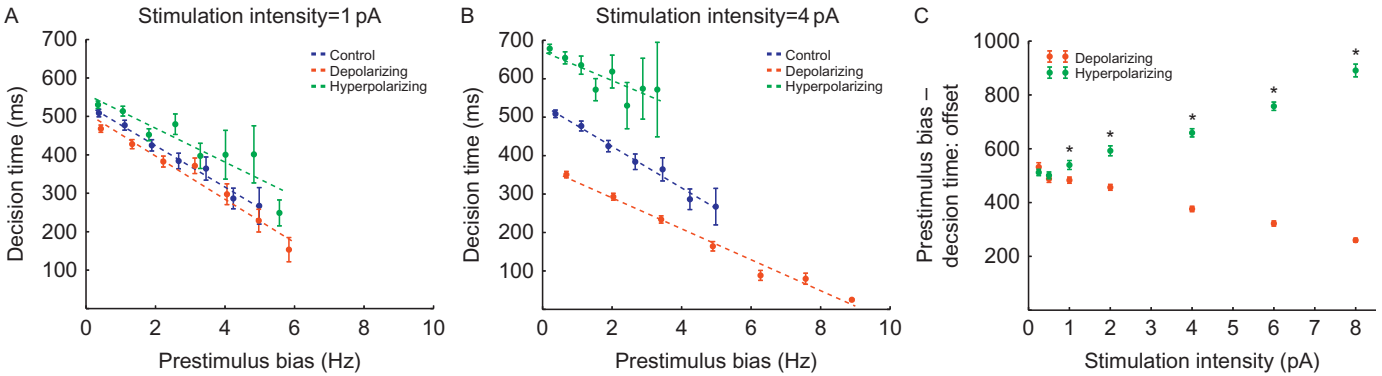

FIGURE 7

Effect of prestimulus bias on decision time. The relationship between the prestimulus bias and decision time at stimulation intensity = 1 pA (A) and 4 pA (B). Decision time and prestimulus bias are negatively correlated, showing that being biased to one option reduces the time the biased pyramidal population takes to reach the threshold firing rate. Higher stimulation intensity results in a greater effect on decision time, but the slope of the relationship between the prestimulus bias and decision time is the same. (C) The difference between the offset of the fitted linear function to prestimulus bias – decision time (stimulation – no stimulation) as a function of stimulation intensity. Asterisks indicate where pairwise comparisons between de- and hyperpolarizing stimulation are significant. The offset monotonically increases with hyperpolarizing stimulation and decreases with depolarizing stimulation. There are no significant changes in the slope with stimulation condition or intensity.

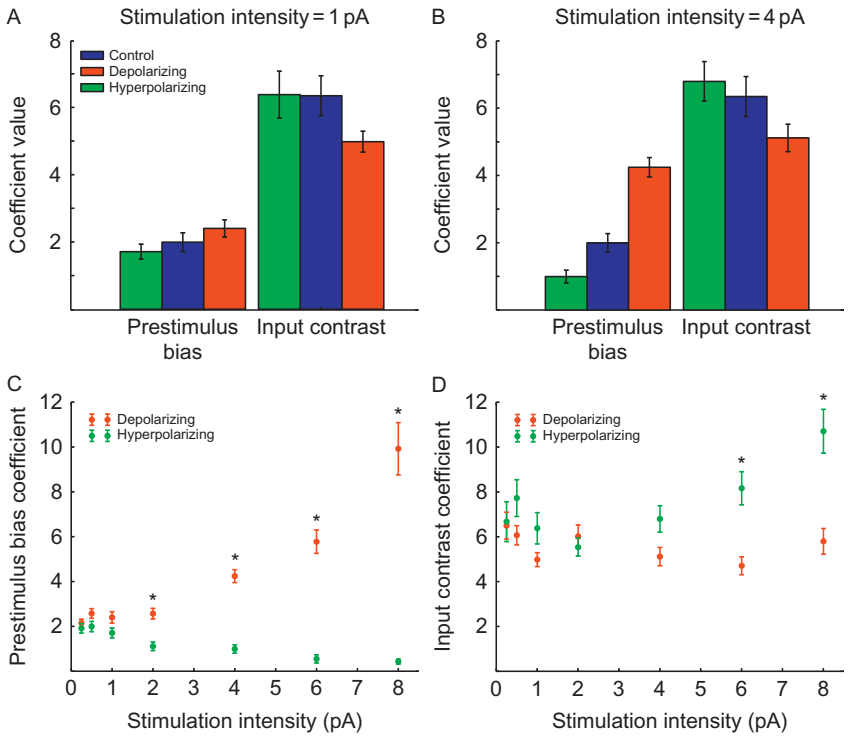

FIGURE 8

Coefficients of logistic regression on accuracy. Coefficients of the logistic regression for the influence of prestimulus bias and input contrast on accuracy at stimulation intensity = 1 pA (A) and 4 pA (B). (C) The prestimulus bias coefficient for stimulation conditions as a function of stimulation intensity. Asterisks indicate where pairwise comparisons between de- and hyperpolarizing stimulation are significant. (D) The input contrast coefficient for stimulation conditions as a function of stimulation intensity.

not strong enough to overcome it. The opposite effect is seen for hyperpolarizing stimulation along with a nonlinear floor effect due to decreasing prestimulus bias with stimulation intensity (Fig. 6). As stimulation intensity increases, the response accuracy in the hyperpolarizing stimulation condition becomes increasingly dependent on the input contrast (Fig. 8D). The difference between the input contrast coefficients for depolarizing and hyperpolarizing stimulation becomes significant at 6 pA, which is also when there is a distinct jump in the percentage of trials with no response during hyperpolarizing stimulation (Fig. 3B). At high intensities of hyperpolarizing stimulation, selection accuracy is dependent on large input contrasts in order to reach the response threshold.

2.5.7 Influence of Prestimulus Bias and Input Contrast on Decision Speed

Another question concerns the relative influence of prestimulus bias and input contrast on decision speed of the network (the inverse of decision time). As shown in Fig. 9A, input contrast contributes more than prestimulus bias to decision speed under all conditions at 1 pA. However, at 4 pA both types of stimulation decrease the relative influence of prestimulus bias, and decrease (depolarizing) or increase (hyperpolarizing) the relative influence of input contrast on decision speed (Fig. 9B). For both types of stimulation, the influence of the prestimulus bias on decision speed reduces to nearly zero with stimulation intensity (Fig. 9C). This is because under high-intensity depolarizing stimulation, the prestimulus bias can become so large that the decision speed is at its upper limit. Therefore, the actual magnitude of the bias has no significant effect on the decision speed. At high levels of

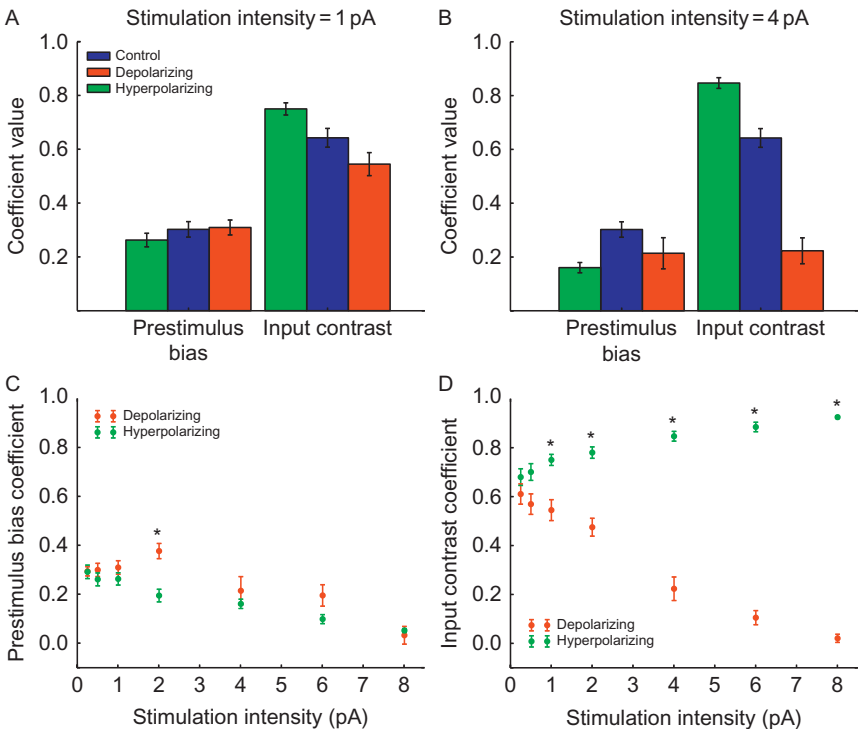

FIGURE 9

Coefficients of linear regression on decision speed. Coefficients of the linear regression for the influence of prestimulus bias and input contrast on decision speed at stimulation intensity = 1 pA (A) and 4 pA (B). (C) The prestimulus bias coefficient for stimulation conditions as a function of stimulation intensity. Asterisks indicate where pairwise comparisons between de- and hyperpolarizing stimulation are significant. (D) The input contrast coefficient for stimulation conditions as a function of stimulation intensity.

prestimulus bias, the input contrast cannot overcome an incorrect bias, and therefore, the influence of the input contrast on decision speed drops steeply (Fig. 9D). With high-intensity hyperpolarizing, the prestimulus bias is reduced to near 0 Hz (Fig. 6), and therefore, the input contrast is the sole factor in determining the decision time, as shown by the increase in the input contrast coefficient with increasing hyperpolarizing stimulation in Fig. 9D.

3 DISCUSSION

NIBS allows for reversible and controlled intervention with the function of neural circuits of the human brain. However, its widespread use and application in basic and translational research starkly contrasts with the dearth of mechanistic and generative models that explain how stimulation alters information processing in neural systems, and how this culminates in behavioral change. There have been steps toward establishing a mechanistic theoretical framework for the effects of tDCS (Ruzzoli et al., 2010), including computational models of its cellular (Rahman et al., 2013) and network-level effects (Molaee-Ardekani et al., 2013). However, to date there have been very few computational models that explain its behavioral effects in terms of neurophysiological dynamics (Douglas et al., 2015). We here present the first computational modeling treatment of nonlinear tDCS effects during a behavioral task that provide detailed hypotheses about the neural causes that lead to observed nonlinear behavioral effects during stimulation.

There are five key observations from our simulations. First, both stimulation types significantly affect both the model's decision time and selection accuracy, and the primary mechanism behind both of these effects is a modulation of the prestimulus difference in the firing rates of the pyramidal populations, which we refer to as prestimulus bias. Second, hyperpolarizing stimulation has a nonlinear reversal effect on accuracy, increasing it at low levels of stimulation intensity by reducing the prestimulus bias, but decreasing accuracy at higher levels because pyramidal populations are so inhibited that it is difficult for them to fire above the response threshold. Third, stimulation decreases (depolarizing) or increases (hyperpolarizing) decision time and has a greater impact on trials with low input contrast (difficult trials). Fourth, there is a nonlinear floor effect of stimulation intensity on decision time with increasing depolarizing stimulation. Fifth, because stimulation was applied throughout the whole trial, the decision time decreases (depolarizing) or increases (hyperpolarizing) beyond the effects accounted for by changes in the prestimulus bias. The nonlinear effects of stimulation intensity on the accuracy and decision time of our model are caused by a limit on the processing speed of the network, nonlinear effects of stimulation on the prestimulus bias, and the inhibitory effect of hyperpolarizing stimulation on pyramidal neurons.

These key observations also immediately highlight that simple sliding-scale rationales are unlikely to be sufficient to conceptualize the impact of tDCS. As we show here, with so-called anodal stimulation, behavioral improvements on decision

time can occur at specific intensity ranges, but the same intervention can lead to decreases in accuracy of performance. Similarly, whether cathodal stimulation improves or impairs behavior may strongly depend on whether accuracy or speed is considered, and furthermore the specific stimulation intensity applied. The issue with conceptual models such as sliding-scale models is that they typically span multiple levels of explanation from neural to regional to behavioral effects without considering the transfer functions between levels (Bestmann et al., 2015). An increase in neural activity, for example, does not imply an increase in processing efficiency (Poldrack, 2014). In other words, biomarkers for the impact of tDCS (e.g., an increase in BOLD activity) do not reveal the underlying mechanism through which stimulation expresses its effects. The present model contains simulated neurons connected in a biologically plausible way and can generate behavioral responses, and is thus able to provide mechanistic hypotheses for why and how nonlinear neural and behavioral effects emerge. This contrasts with conceptual models which may seek to be mechanistic in the sense that they are logically coherent, whereas the approach used here is mechanistic by providing an explanation of phenomena by reference to physical or biological causes.

We tested two types of stimulation, depolarizing (anodal) and hyperpolarizing (cathodal), and varied the intensity of each type within the ranges resulting from typical application of tDCS to determine the relationship between stimulation strength and various neural and behavioral measures. In our simulations, interneurons were also affected by stimulation, but the results were qualitatively similar in additional simulations in which stimulation was only applied to the pyramidal populations. Both stimulation types significantly affected both the model's decision time and selection accuracy. An analysis of the model's neural dynamics and their relationship to these behavioral measures revealed that the primary mechanism behind both of these effects was a modulation of the prestimulus difference in the firing rates of the pyramidal populations, which we refer to as prestimulus bias.

Prestimulus bias was caused by noisy variations in the background input projecting to all neural populations and was enhanced by depolarizing and suppressed by hyperpolarizing stimulation. tDCS therefore effectively increases (depolarizing) or decreases (hyperpolarizing) the effects of the noisy background input on the selection process. Prestimulus bias has a natural lower level of zero when both pyramidal populations are firing at the same rate, which causes a nonlinear floor effect of hyperpolarizing stimulation intensity on the prestimulus bias as this limit is approached. As the prestimulus bias decreases, randomness in the selection is increasingly driven by the variability in the task-related inputs. These simulations predict that for neural attractor networks, the effect of stimulation is not simply an increase or decrease of noise (Miniussi et al., 2013), but a modulation of the effects of the noise on the selection process.

The mean effect of stimulation on the prestimulus bias increased with increasing stimulation intensity. This decreased accuracy with depolarizing stimulation because it enhanced the prestimulus bias, increasing the influence of noisy background input on the selection. Hyperpolarizing stimulation had a nonlinear reversal effect on

accuracy. At low levels, increasing hyperpolarizing stimulation intensity improved accuracy by reducing the prestimulus bias, which could be the explanation for performance improvements observed with low-intensity hyperpolarizing stimulation in a similar task (Antal et al., 2004). However beyond a certain level of intensity, in our model hyperpolarizing stimulation decreased accuracy because pyramidal populations were so inhibited that it was difficult for them to fire above the response threshold. This could explain why studies with hyperpolarizing stimulation intensities greater than 1 mA find performance decreases (Berryhill et al., 2010; Loui et al., 2010; Stone and Tesche, 2009).

The prestimulus bias influenced decision time by moving the firing rate of the biased pyramidal population closer to or further from the response threshold. In our simulations, stimulation decreased (depolarizing) or increased (hyperpolarizing) decision time and had a greater impact on trials with low input contrast (difficult trials). There is a lower bound on decision time which is determined by the neural time constant and axonal delay parameters that regulate the rate at which the firing rate of a neural population can increase. This causes a nonlinear floor effect of stimulation intensity on decision time as the model's performance approaches this boundary with increasing depolarizing stimulation. This effect has been found with increasing depolarizing stimulation intensity in a working memory task (Hoy et al., 2013; Teo et al., 2011).

While stimulation influenced decision time by modulating the prestimulus bias, its effects also extended beyond the onset of the task-related inputs. In all conditions, the decision time linearly decreased with increasing prestimulus bias. While the slope of this relationship did not vary with stimulation type or intensity, the offset increased with hyperpolarizing stimulation intensity and decreased with depolarizing stimulation intensity. This change in offset reflects the fact that the stimulation continued through the whole trial and increased (depolarizing) or decreased (hyperpolarizing) the rate of the rise in firing rate of the winning pyramidal population.

The use of *in silico* interrogation of neural systems inevitably requires assumptions and uses mesoscopic approximations of underlying complex microstructure. We do not claim that the present model provides ground truth with regard to the underlying mechanism of nonlinear tDCS effects. However, the example introduced here provides a useful stepping stone for future use of mesoscopic models: first, the neural network used here is an established model that accurately predicts subject's choice behavior, as well as large-scale population signals as recorded with fMRI or MEG (Bonaiuto and Arbib, 2014; Hunt et al., 2012; Wang, 2008). Second, the model provides a mesoscopic level of description regarding the neural causes that generate behavior, which reduces the tractability of the problem but not at the expense of being biophysical plausible. Finally, we note that there is now a rich panoply of models for many behaviors at these levels of description (Arbib, 1995; Christopoulos et al., 2015; Trappenberg, 2009), thus allowing for the interrogation of the impact of NIBS in such systems, without the requirement of a strong intellectual investment in any of these models.

Moreover, we note that there is sufficient uncertainty with regard to the precise neural elements targeted by any form of NIBS. For example, for tDCS, it remains unknown to which degree neurons of different morphology might be affected. While *in vitro* studies provide invaluable insight on how polarization interacts with single neurons (Chan & Nicholson, 1986; Radman et al., 2009), how polarized networks of neurons, potentially of different types as in the examples presented here, respond to tDCS remains largely unknown. Finally, the physiological impact of tDCS even on single neurons is likely complex, and simply simulating tDCS through changes in membrane polarization may not account for this complexity. However, one key advantage of computational neurostimulation is that competing hypotheses about the mechanism of action of tDCS can directly be compared without major expense, and the resulting predictions can be submitted to experimental validation. While the predictions generated by our simulations have yet to be verified experimentally, the framework detailed above can provide a blueprint for future work on the neural and behavioral consequences of NIBS.

ACKNOWLEDGMENT

S.B. and J.J.B. were supported by the European Research Council (ERC; ActSelectContext 260424).

REFERENCES

Antal, A., Nitsche, M.A., Kruse, W., Kincses, T.Z., Hoffmann, K.-P., Paulus, W., 2004. Direct current stimulation over V5 enhances visuomotor coordination by improving motion perception in humans. J. Cogn. Neurosci. 16, 521–527.

Arbib, M., 1995. The Handbook of Brain Theory and Neural Networks. MIT Press, Cambridge, MA.

Batsikadze, G., Moliadze, V., Paulus, W., Kuo, M.-F., Nitsche, M.A., 2013. Partially nonlinear stimulation intensity-dependent effects of direct current stimulation on motor cortex excitability in humans. J. Physiol. 591, 1987–2000.

Berryhill, M.E., Wencil, E.B., Branch Coslett, H., Olson, I.R., 2010. A selective working memory impairment after transcranial direct current stimulation to the right parietal lobe. Neurosci. Lett. 479, 312–316.

Bestmann, S., de Berker, A.O., Bonaiuto, J., 2015. Understanding the behavioural consequences of noninvasive brain stimulation. Trends Cogn. Sci. 19 (1), 13–20.

Bikson, M., Inoue, M., Akiyama, H., Deans, J.K., Fox, J.E., Miyakawa, H., Jefferys, J.G.R., 2004. Effects of uniform extracellular DC electric fields on excitability in rat hippocampal slices in vitro. J. Physiol. 557, 175–190.

Bikson, M., Rahman, A., Datta, A., 2012. Computational models of transcranial direct current stimulation. Clin. EEG Neurosci. 43, 176–183.

Bindman, L.J., Lippold, O.C.J., Redfearn, J.W.T., 1964. The action of brief polarizing currents on the cerebral cortex of the rat (1) during current flow and (2) in the production of long-lasting after-effects. J. Physiol. 172, 369–382.

Bonaiuto, J., Arbib, M.A., 2010. Extending the mirror neuron system model, II: what did I just do? A new role for mirror neurons. Biol. Cybern. 102, 341–359.
Bonaiuto, J., Arbib, M.A., 2014. Modeling the BOLD correlates of competitive neural dynamics. Neural Netw. 49, 1–10.
Braitenberg, V., Schüz, A., 1991. Anatomy of the Cortex: Statistics and Geometry. Springer-Verlag Publishing, New York.
Brette, R., Gerstner, W., 2005. Adaptive exponential integrate-and-fire model as an effective description of neuronal activity. J. Neurophysiol. 94, 3637–3642.
Camperi, M., Wang, X.-J., 1998. A model of visuospatial working memory in prefrontal cortex: recurrent network and cellular bistability. J. Comput. Neurosci. 5, 383–405.
Chan, C.Y., Nicholson, C., 1986. Modulation by applied electric fields of Purkinje and stellate cell activity in the isolated turtle cerebellum. J. Physiol. 371, 89–114.
Christopoulos, V., Bonaiuto, J., Andersen, R.A., 2015. A biologically plausible computational theory for value integration and action selection in decisions with competing alternatives. PLoS Computat. Biol. 11 (3), e1004104.
Compte, A., Brunel, N., Goldman-rakic, P.S., Wang, X., 2000. Synaptic mechanisms and network dynamics underlying spatial working memory in a cortical network model. Cereb. Cortex 10, 910–923.
Datta, A., Truong, D., Minhas, P., Parra, L.C., Bikson, M., 2012. Inter-individual variation during transcranial direct current stimulation and normalization of dose using MRI-derived computational models. Front. Psychiatry 3, 91.
De Berker, A.O., Bikson, M., Bestmann, S., 2013. Predicting the behavioral impact of transcranial direct current stimulation: issues and limitations. Front. Hum. Neurosci. 7, 613.
Deco, G., Rolls, E.T., 2005. Neurodynamics of biased competition and cooperation for attention: a model with spiking neurons. J. Neurophysiol. 94 (1), 295–313.
Douglas, Z.H., Maniscalco, B., Hallett, M., Wassermann, E.M., He, B.J., 2015. Modulating conscious movement intention by noninvasive brain stimulation and the underlying neural mechanisms. J. Neurosci. 35, 7239–7255.
Fritsch, B., Reis, J., Martinowich, K., Schambra, H.M., Ji, Y., Cohen, L.G., Lu, B., 2010. Direct current stimulation promotes BDNF-dependent synaptic plasticity: potential implications for motor learning. Neuron 66, 198–204.
Funke, K., 2013. Quite simple at first glance—complex at a second: modulating neuronal activity by tDCS. J. Physiol. 591, 3809.
Goodman, D., Brette, R., 2008. Brian: a simulator for spiking neural networks in python. Front. Neuroinform. 2, 5.
Hestrin, S., Sah, P., Nicoll, R.A., 1990. Mechanisms generating the time course of dual component excitatory synaptic currents recorded in hippocampal slices. Neuron 5, 247–253.
Hoy, K.E., Emonson, M.R.L., Arnold, S.L., Thomson, R.H., Daskalakis, Z.J., Fitzgerald, P.B., 2013. Testing the limits: investigating the effect of tDCS dose on working memory enhancement in healthy controls. Neuropsychologia 51, 1777–1784.
Hunt, L.T., Kolling, N., Soltani, A., Woolrich, M.W., Rushworth, M.F.S., Behrens, T.E.J., 2012. Mechanisms underlying cortical activity during value-guided choice. Nat. Neurosci. 15 (470–6), S1–S3.
Itti, L., Koch, C., 2001. Computational modelling of visual attention. Nat. Rev. Neurosci. 2, 194–203.

Iyer, M.B., Mattu, U., Grafman, J., Lomarev, M., Sato, S., Wassermann, E.M., 2005. Safety and cognitive effect of frontal DC brain polarization in healthy individuals. Neurology 64, 872–875.

Izhikevich, E.M., 2006. Polychronization: computation with spikes. Neural Comput. 18, 245–282.

Jahr, C., Stevens, C., 1990. A quantitative description of NMDA receptor-channel kinetic behavior. J. Neurosci. 10, 1830–1837.

Krause, B., Márquez-Ruiz, J., Kadosh, R.C., 2013. The effect of transcranial direct current stimulation: a role for cortical excitation/inhibition balance? Front. Hum. Neurosci. 7, 602.

Kuo, H.-I., Bikson, M., Datta, A., Minhas, P., Paulus, W., Kuo, M.-F., Nitsche, M.A., 2013. Comparing cortical plasticity induced by conventional and high-definition 4×1 ring tDCS: a neurophysiological study. Brain Stimul. 6, 644–648.

Liu, F., Wang, X.J., 2008. A common cortical circuit mechanism for perceptual categorical discrimination and veridical judgment. PLoS Comput. Biol. 4 (12), e1000253.

Lo, C.-C., Wang, X.-J., 2006. Cortico-basal ganglia circuit mechanism for a decision threshold in reaction time tasks. Nat. Neurosci. 9, 956–963.

Loui, P., Hohmann, A., Schlaug, G., 2010. Inducing disorders in pitch perception and production: a reverse-engineering approach. Proc. Meet. Acoust. 9, 50002.

Mayor, J., Gerstner, W., 2005. Noise-enhanced computation in a model of a cortical column. Neuroreport 16, 1237–1240.

Miniussi, C., Harris, J.A., Ruzzoli, M., 2013. Modelling non-invasive brain stimulation in cognitive neuroscience. Neurosci. Biobehav. Rev. 37, 1702–1712.

Molaee-Ardekani, B., Márquez-Ruiz, J., Merlet, I., Leal-Campanario, R., Gruart, A., Sánchez-Campusano, R., Birot, G., Ruffini, G., Delgado-García, J.-M., Wendling, F., 2013. Effects of transcranial direct current stimulation (tDCS) on cortical activity: a computational modeling study. Brain Stimul. 6, 25–39.

Monte-Silva, K., Kuo, M.-F., Hessenthaler, S., Fresnoza, S., Liebetanz, D., Paulus, W., Nitsche, M.A., 2013. Induction of late LTP-like plasticity in the human motor cortex by repeated non-invasive brain stimulation. Brain Stimul. 6, 424–432.

Nitsche, M.A., Paulus, W., 2000. Excitability changes induced in the human motor cortex by weak transcranial direct current stimulation. J. Physiol. 527, 633–639.

Nitsche, M.A., Paulus, W., 2011. Transcranial direct current stimulation—update 2011. Restor. Neurol. Neurosci. 29, 463–492.

Ohn, S.H., Park, C.-I., Yoo, W.-K., Ko, M.-H., Choi, K.P., Kim, G.-M., Lee, Y.T., Kim, Y.-H., 2008. Time-dependent effect of transcranial direct current stimulation on the enhancement of working memory. Neuroreport 19, 43–47.

Palmer, J., Huk, A.C., Shadlen, M.N., 2005. The effect of stimulus strength on the speed and accuracy of a perceptual decision. J. Vis. 5, 376–404.

Paulus, W., Peterchev, A.V., Ridding, M., 2013. Transcranial electric and magnetic stimulation: technique and paradigms. Handb. Clin. Neurol. 116, 329–342.

Poldrack, R.A., 2014. Is "efficiency" a useful concept in cognitive neuroscience? Dev. Cogn. Neurosci. 11, 12–17.

Radman, T., Ramos, R.L., Brumberg, J.C., Bikson, M., 2009. Role of cortical cell type and morphology in subthreshold and suprathreshold uniform electric field stimulation in vitro. Brain Stimul. 2 (215–28), 228.

Rahman, A., Reato, D., Arlotti, M., Gasca, F., Datta, A., Parra, L.C., Bikson, M., 2013. Cellular effects of acute direct current stimulation: somatic and synaptic terminal effects. J. Physiol. 591, 2563–2578.

R Development Core Team, 2011. The R Project for Statistical Computing.

Riesenhuber, M., Poggio, T., 2000. Models of object recognition. Nat. Neurosci. 3, 1199–1204.

Ruzzoli, M., Marzi, C.A., Miniussi, C., 2010. The neural mechanisms of the effects of transcranial magnetic stimulation on perception. J. Neurophysiol. 103, 2982–2989.

Salin, P.A., Prince, D.A., 1996. Spontaneous GABAA receptor-mediated inhibitory currents in adult rat somatosensory cortex. J. Neurophysiol. 75, 1573–1588.

Shekhawat, G.S., Stinear, C.M., Searchfield, G.D., 2013. Transcranial direct current stimulation intensity and duration effects on tinnitus suppression. Neurorehabil. Neural Repair 27, 164–172.

Spruston, N., Jonas, P., Sakmann, B., 1995. Dendritic glutamate receptor channels in rat hippocampal CA3 and CA1 pyramidal neurons. J. Physiol. 482, 325–352.

Stone, D.B., Tesche, C.D., 2009. Transcranial direct current stimulation modulates shifts in global/local attention. Neuroreport 20, 1115–1119.

Swadlow, H.A., 1990. Efferent neurons and suspected interneurons in S-1 forelimb representation of the awake rabbit: receptive fields and axonal properties. J. Neurophysiol. 63, 1477–1498.

Swadlow, H.A., 1994. Efferent neurons and suspected interneurons in motor cortex of the awake rabbit: axonal properties, sensory receptive fields, and subthreshold synaptic inputs. J. Neurophysiol. 71, 437–453.

Teo, F., Hoy, K.E., Daskalakis, Z.J., Fitzgerald, P.B., 2011. Investigating the role of current strength in tDCS modulation of working memory performance in healthy controls. Front. Psychiatry 2, 45.

Trappenberg, T., 2009. Fundamentals of Computational Neuroscience. Oxford University Press, Oxford, England.

Wang, X.-J., 2002. Probabilistic decision making by slow reverberation in cortical circuits. Neuron 36, 955–968.

Wang, X.-J., 2008. Decision making in recurrent neuronal circuits. Neuron 60, 215–234.

Wilson, H.R., Cowan, J.D., 1972. Excitatory and inhibitory interactions in localized populations of model neurons. Biophys. J. 12, 1–24.

Wolpert, D.M., Ghahramani, Z., 2000. Computational principles of movement neuroscience. Nat. Neurosci. Neurosci. 3, 1212–1217.

Xiang, Z., Huguenard, J.R., Prince, D.A., 1998. GABAA receptor-mediated currents in interneurons and pyramidal cells of rat visual cortex. J. Physiol. 506, 715–730.